

# Anomalous thermal expansion and chiral phonons in $\text{BiB}_3\text{O}_6$

Carl P. Romao<sup>1,2,\*</sup>

<sup>1</sup>*Department of Chemistry, University of Oxford,  
Inorganic Chemistry Laboratory, South Parks Road, Oxford OX1 3QR, UK*

<sup>2</sup>*Section for Solid State and Theoretical Inorganic Chemistry,  
Institute of Inorganic Chemistry, University of Tübingen,  
Auf der Morgenstelle 18, D-72076 Tübingen, Germany*

(Dated: June 13, 2022)

The origins of anomalous thermal expansion in the chiral monoclinic solid  $\alpha\text{-BiB}_3\text{O}_6$  have been studied through *ab initio* calculations. Positive and negative axial thermal expansion are shown to be driven by librations of borate units, elastic anisotropy, and most notably by chiral acoustic phonons involving elliptical revolutions of bismuth atoms. The chirality of the lattice gives rise to these modes by allowing the transverse acoustic branches to have opposite circular polarizations, only one of which couples strongly to the lattice strains. This result furthers understanding of relationships between crystallographic symmetry and physical properties.

The monoclinic  $\alpha$  phase of bismuth borate ( $\text{BiB}_3\text{O}_6$ ) (Fig. 1), in addition to having promising applications in nonlinear optics [1, 2] and quantum computing [3, 4], possesses the unusual physical properties of uniaxial negative thermal expansion (NTE) [5, 6] and negative linear compressibility [7, 8]. The chiral  $C2$  space group adopted by  $\alpha\text{-BiB}_3\text{O}_6$  [6] has unusually low symmetry for an NTE material [9, 10], or indeed more generally for an inorganic solid. The chirality of  $\alpha\text{-BiB}_3\text{O}_6$  permits it to have chiral phonons, *i.e.*, phonons with a circular polarization and pseudoangular momentum [11–13]. Phonon chirality has been shown to affect the anharmonic properties of phonons through the phonon Hall effect [11], and through modification of symmetry constraints for scattering [14], but connections to the related anharmonic property of thermal expansion [15] have not previously been explored.

thermal expansion along **b** [5, 6]. Anisotropic thermal expansion, common among borate nonlinear optical materials [16], causes difficulties in the growth of single crystals and their use in applications [5, 17]. Recently, significant attention has been paid to materials which display NTE along one or two lattice vectors due to, for example, anomalously large-magnitude thermal expansion [18], connections with other physical properties, such as ferroelectricity [19, 20], or the use of chemical control to achieve zero thermal expansion [21]. Axial NTE is relatively common in framework materials of the tetragonal, orthorhombic, and hexagonal crystal families, *i.e.*, those families whose thermal expansion tensors have one or two unique non-zero elements [9, 10]. In these crystal families, elastic anisotropy can combine with symmetry constraints to yield anisotropic thermal expansion, with positive thermal expansion and negative thermal expansion each found along at least one axis [22].

Negative thermal expansion is extremely rare in materials with monoclinic and triclinic crystal lattices [9, 10]. Outside of  $\alpha\text{-BiB}_3\text{O}_6$ , the examples which have been reported are isolated to molecular solids, where the mechanism commonly involves the sliding of layers relative to each other [23, 24]. The general absence of NTE in monoclinic framework solids has several potential origins. The vibrational origins of NTE have often been related to symmetry-lowering phase transitions, as the soft modes which cause these transitions have negative Grüneisen parameters [10, 25]. Materials which possess low-symmetry lattices are less likely to have these transitions available. Additionally, the symmetry constraints on the thermal expansion tensor are significantly weaker for monoclinic and triclinic systems, as thermal expansion maxima and minima are not required to be co-aligned with the lattice vectors [22]. Because of this rarity, a study of the vibrational origins of NTE in a monoclinic system has not previously been reported.

Herein is reported a computational study of thermal expansion in  $\alpha\text{-BiB}_3\text{O}_6$ , conducted with the goal of iden-

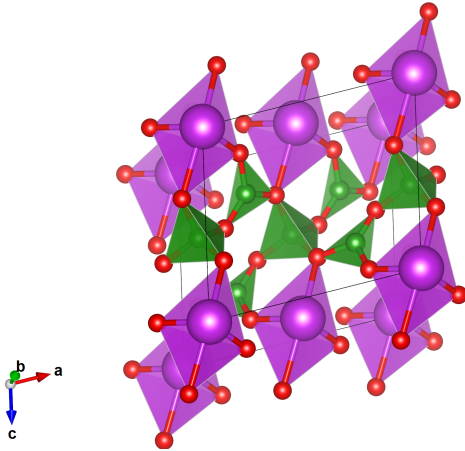


FIG. 1. The structure of  $\alpha\text{-BiB}_3\text{O}_6$  [6], with bismuth atoms coloured in magenta, oxygen atoms coloured in red, and boron atoms coloured in green. The view is along **b**.

The thermal expansion of  $\alpha\text{-BiB}_3\text{O}_6$  is highly anisotropic, with large NTE along **a** and large positive

tifying the origins of NTE in this low-symmetry material and identifying potential connections with phonon chirality. Calculations were performed using the density functional theory software package ABINIT [26–29]; example input files are available as part of the Supplemental Material [30]. Phonon band structures and the elastic tensor were calculated using density functional perturbation theory [31, 32]. Variations in phonon energies as a function of uniaxial stress determined directional mode Grüneisen parameters ( $\gamma_{ij,n,\mathbf{k}}$ ) by [22]:

$$\gamma_{ij,n,\mathbf{k}} = -\frac{1}{s_{ijij}} \left( \frac{\partial \ln \omega_{n,\mathbf{k}}}{\partial \sigma_{ij}} \right)_{T,\sigma'}, \quad (1)$$

where  $\mathbf{s}$  is the elastic compliance tensor. These mode Grüneisen parameters were averaged, weighted by their contribution to the heat capacity ( $C_e$ ), to give bulk Grüneisen parameters ( $\gamma_{ij}$ ), and subsequently used to determine directional coefficients of thermal expansion (CTEs,  $\alpha_{ij}$ ) as follows [22]:

$$\alpha_{ij} = s_{ijij} \gamma_{ij} \frac{C_e}{V}. \quad (2)$$

The uniaxial stress perturbations used were  $\sigma_{11}$ ,  $\sigma_{22}$ ,  $\sigma_{33}$ , and  $\sigma_{13}$ ; the Cartesian axes  $\mathbf{x}$  and  $\mathbf{y}$  coincide with the lattice vectors  $\mathbf{a}$  and  $\mathbf{b}$ , respectively, and the  $\mathbf{z}$  axis is therefore the stacking direction of the borate layers (see Fig. 1).

Computational methods were validated by comparison of calculated elastic tensors and thermal expansion tensors to experimental values [5, 7]. As described in the Supplemental Material [30], several approaches were trialled [33–41]. The most accurate results were found for a dispersion-corrected exchange–correlation functional [35, 36]; as shown in Table I the calculations underestimated the magnitude of thermal expansion but were able to qualitatively reproduce the experimental behaviour.

TABLE I. Calculated elements of the thermal expansion tensor at 300 K (in  $10^{-6} \text{ K}^{-1}$ ) of  $\alpha\text{-BiB}_3\text{O}_6$ , compared to the experimental result of Ref. 5.

Element	Calculated	Experimental [5]
$\alpha_{11}$	−7.5	−25.6
$\alpha_{22}$	8.1	50.4
$\alpha_{33}$	5.2	7.7
$\alpha_{13}$	−10.2	−5.33

The calculated directional Young’s moduli are shown in Fig. 2, and phonon band structures, coloured by their directional mode Grüneisen parameters ( $\gamma_{ij}$ ), are shown in Fig. 3. Thermal expansion is driven by acoustic bands and low-energy optic bands, predominantly those with energies below  $200 \text{ cm}^{-1}$ . While understanding of the origins of NTE has often focused on the low-energy optic phonons corresponding to rigid unit modes, acoustic

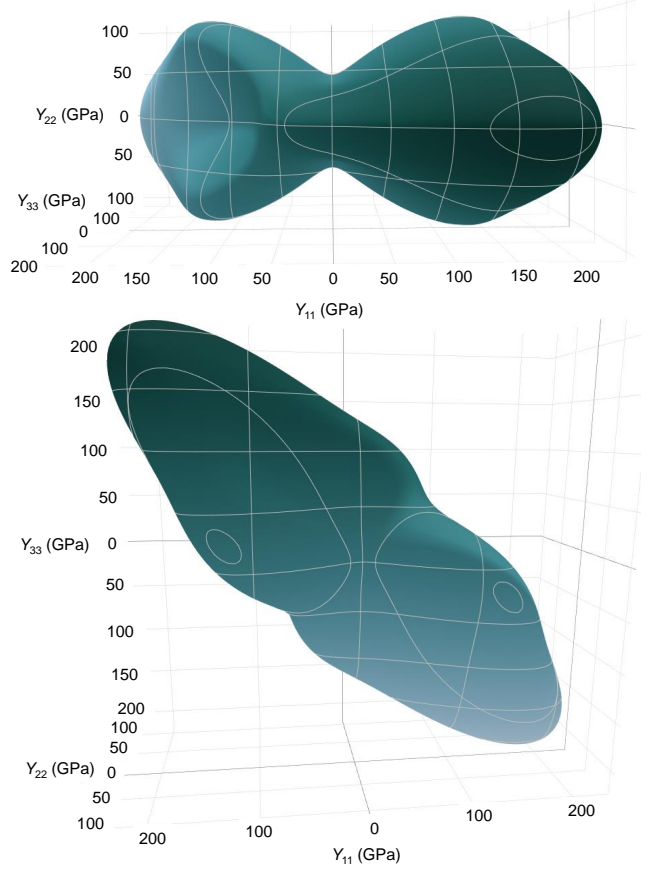


FIG. 2. Calculated directional Young’s modulus ( $Y_{ii}$ ) of  $\alpha\text{-BiB}_3\text{O}_6$ , shown as a blue surface. Visualization generated with ELATE [42].

modes are often also significant contributors [10, 43, 44], as is seen here. The small mode Grüneisen parameters for perturbations along  $\mathbf{b}$  ( $\gamma_{22}$ ) indicate that the large thermal expansion in this direction is driven by elastic anisotropy, as the directional thermal expansion is inversely proportional to the directional Young’s modulus ( $Y_{ii} = 1/s_{iiii}$ , see Eq. 2) and the directional Young’s modulus is minimal along  $\mathbf{b}$  (Fig. 2). Indeed, in the  $\mathbf{ab}$  plane the directional Young’s modulus of  $\alpha\text{-BiB}_3\text{O}_6$  exhibits the bowtie shape characteristic of framework materials with highly anisotropic thermal expansion [22, 45–47].

The origins of anomalous thermal expansion in  $\alpha\text{-BiB}_3\text{O}_6$  can be understood further by inspection of the eigenvectors of the modes with large mode Grüneisen parameters. These are available as part of the Supplemental Material [30], in a format which allows their visualization in animated form [49]. The eigenvectors of several modes which are notable contributors to the thermal expansion are shown in Fig. 4.

Thermal expansion in  $\alpha\text{-BiB}_3\text{O}_6$  is driven primarily by two types of low-energy phonons: those which involve

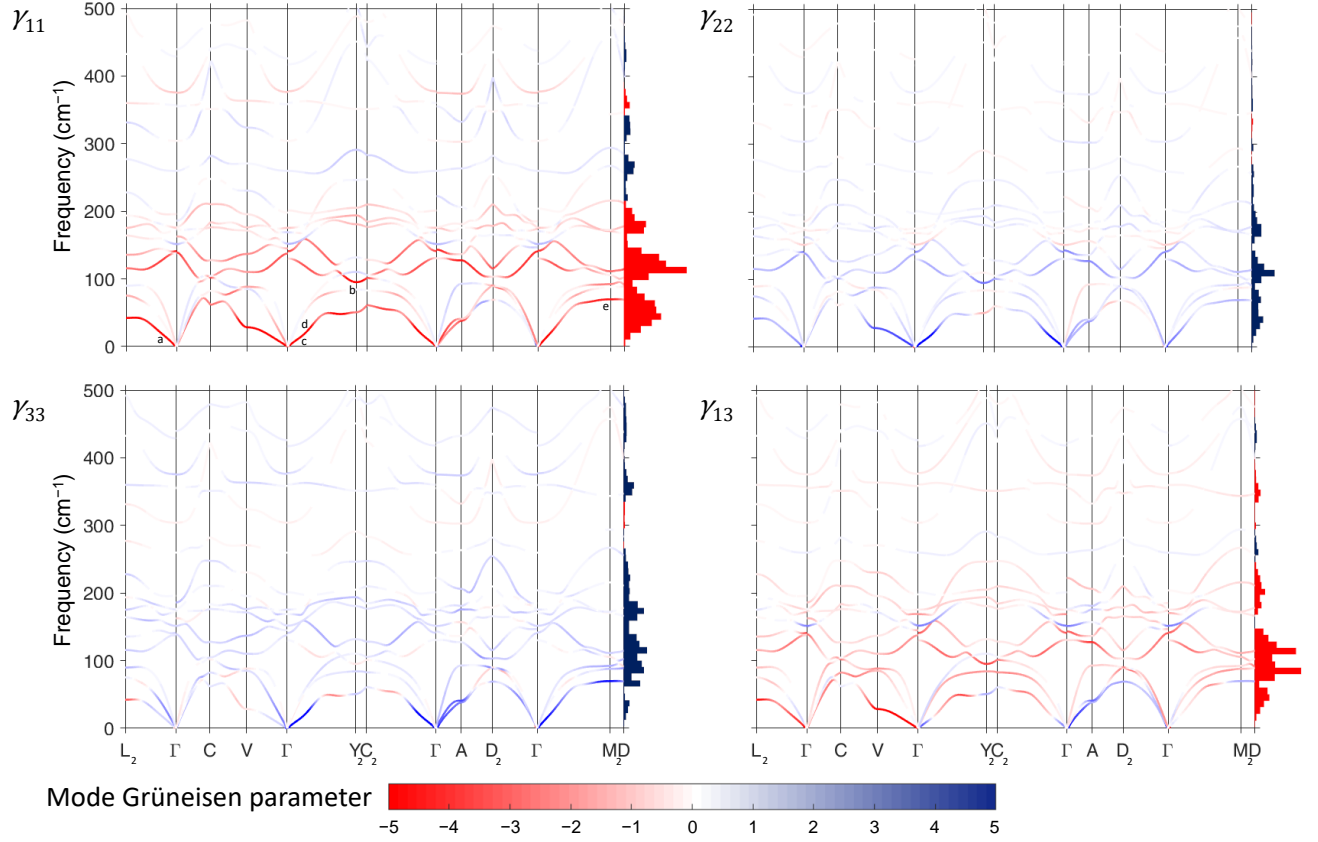


FIG. 3. Phonon band structure of  $\alpha$ - $\text{BiB}_3\text{O}_6$ , with bands coloured according to their directional mode Grüneisen parameters ( $\gamma_{ij,n,\mathbf{k}}$ ), calculated using the method of Ref. 22. Phonons with energies greater than  $500 \text{ cm}^{-1}$  do not contribute significantly to thermal expansion and are not shown. The density of states ( $\rho$ ), weighted by the Grüneisen parameters as  $\sum_{\mathbf{k}} \rho_{\mathbf{k}}(\omega) \gamma_{ij,\mathbf{k}}(\omega)$ , is shown as a histogram at the right of each plot, with positive values coloured in blue and negative values in red. Special points in the Brillouin zone were selected following Ref. 48. The modes marked a–e are visualized in Fig. 4.

large displacements of the Bi atoms (*e.g.*, Fig. 4 a, c and d), and those which primarily involve motions of rigid  $\text{BO}_3$  triangles and  $\text{BO}_4$  tetrahedra (*e.g.*, Fig. 4 b and e). The modes in this latter group involve rocking of the oxygen atoms involved in either the B–O–B bonds (Fig. 4 c) or the Bi–O–B bonds (Fig. 4 d). Such librations of bridging atoms are known to be a common mechanism for NTE in flexible framework materials [9, 10]. Indeed, inspection of the directional Young’s modulus (Fig. 2) indicates that, despite its layered structure,  $\alpha$ - $\text{BiB}_3\text{O}_6$  behaves elastically like a flexible framework: it has a mixture of compliant directions ( $[1\ 0\ 0]$ ,  $[0\ 1\ 0]$ , and  $[1\ 0\ -1]$ ) and stiff directions ( $[1\ 1\ 0]$ ,  $[-1\ 1\ 0]$ , and  $[0\ 0\ 1]$ ).

The low energy acoustic phonons which drive positive thermal expansion along **b**, and contribute significantly to negative thermal expansion along **a**, involve large displacements of the Bi atoms as well as smaller transverse motions of the borate framework. These phonons can be divided into two categories; the first being modes where the Bi atom oscillates along a linear trajectory (*e.g.* Fig. 4 a). The second category is comprised of modes where

the Bi atoms orbit their average positions (*e.g.* Fig. 4 c). These orbits are elliptical due to the anisotropic coordination environment of the Bi atoms (see Fig. 1). These modes are chiral; as Fig. 4 shows the coordinated rotation of the bismuth atoms has a distinct handedness and a circular polarization results.

The circular polarization of a phonon (**S**) can be quantified by performing a series of basis transformations to its eigenvectors ( $|\epsilon\rangle$ ) so that each sublattice has a right- or left-handed circular polarization with respect to a given axis [11]. This method has previously been applied to two-dimensional materials [11, 12]; to examine the chiralities of the phonons in  $\alpha$ - $\text{BiB}_3\text{O}_6$  it was generalized by determining the polarization along each of the Cartesian axes independently. The new bases are defined, for example for a polarization along **b**, as:  $|R_{1,22}\rangle \equiv \frac{1}{\sqrt{2}}(i\ 0\ 1\ \cdots\ 0)^T$ ,  $|L_{1,22}\rangle \equiv \frac{1}{\sqrt{2}}(-i\ 0\ 1\ \cdots\ 0)^T$ ,  $|R_{n,22}\rangle \equiv \frac{1}{\sqrt{2}}(0\ \cdots\ i\ 0\ 1)^T$ , and  $|L_{n,22}\rangle \equiv \frac{1}{\sqrt{2}}(0\ \cdots\ -i\ 0\ 1)^T$ , where  $n$  is the number of atoms [11, 12]. The phonon polarization along **b** ( $S_{22}$ ) is then the sum of the polar-

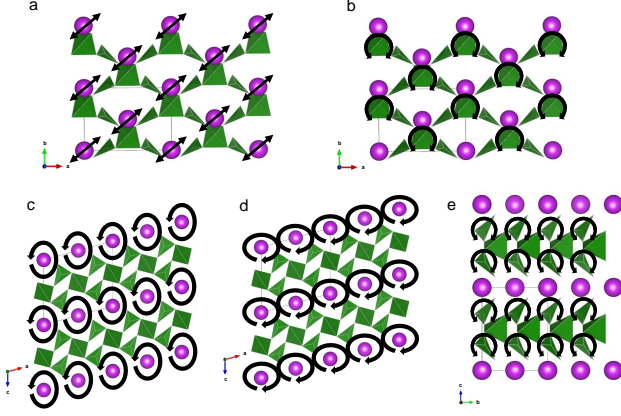


FIG. 4. Cartoon view of the eigenvectors of several phonons in  $\alpha$ - $\text{BiB}_3\text{O}_6$ . a: low-energy transverse acoustic mode in the  $\Gamma \rightarrow \text{L}$  direction; b: optic mode at  $\text{Y}_2$ ; c: low-energy transverse acoustic mode in the  $\Gamma \rightarrow \text{Y}_2$  direction; d: high-energy transverse acoustic mode in the  $\Gamma \rightarrow \text{Y}_2$  direction; e: low-energy transverse acoustic mode at  $\text{M}_2$  (see Fig. 3). See the Supplemental Material for animations of these modes [30].

izations of each sublattice:

$$S_{22} = \sum_{\alpha=1}^n (|\langle R_{\alpha,22} | \epsilon \rangle|^2 - |\langle L_{\alpha,22} | \epsilon \rangle|^2) \hbar; \quad (3)$$

the circular polarizations  $S_{11}$  and  $S_{33}$  are obtained simply by rotation of the basis vectors [11, 12].

The circular polarizations of the low-energy phonons along  $\mathbf{y}$  are shown in Fig. 5 (the polarizations along  $\mathbf{x}$  and  $\mathbf{z}$  are shown in the Supplemental Material [30]). Comparison of Fig. 3 and Fig. 5 shows that phonon chirality can significantly influence the mode Grüneisen parameters. The transverse acoustic branches, for example along  $\Gamma \rightarrow \text{C}_2$ , can have opposite chirality, with one branch involving right-handed revolutions of Bi atoms (Fig. 4 c) and the other having left-handed motions (Fig. 4 d). The right-handed branch couples strongly to the lattice strains, as evidenced by its large mode Grüneisen parameters, while the left-handed branch does not couple significantly. Note that the two branches do not simply mirror each other; branches with the same energies but reversed chirality exist along paths related by time-reversal symmetry, *e.g.*  $\Gamma \rightarrow \text{C}'_2$  [11, 48]. Specific signs of the phonon polarization do not lead to specific mode Grüneisen parameters; the chirality is important in that the polarized modes correspond to motions which would be symmetry-forbidden for phonon eigenvectors in an achiral lattice.

Comparison of Fig. 3 and Fig. 5 indicates that the acoustic modes with circular polarization along  $\mathbf{b}$  are significant contributors to the anomalous thermal expansion of  $\alpha$ - $\text{BiB}_3\text{O}_6$ , as they have large values of  $\gamma_{11}$ ,  $\gamma_{22}$ , and  $\gamma_{33}$ . These mode Grüneisen parameters are significantly influenced by dispersive interactions, as their signs and

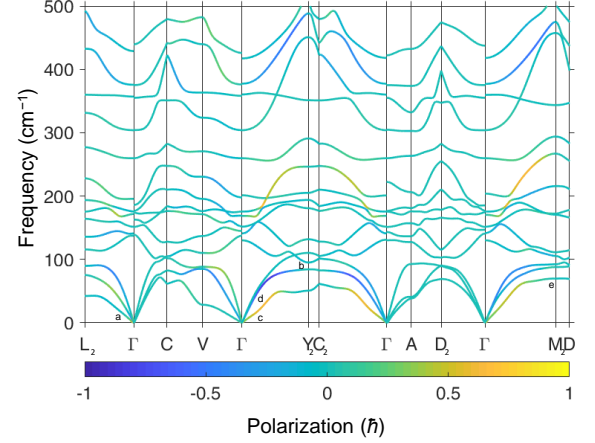


FIG. 5. Phonon band structure of  $\alpha$ - $\text{BiB}_3\text{O}_6$ , with bands coloured according to their circular polarizations along  $\mathbf{b}$  ( $S_{22}$ ). A polarization of  $\hbar$  corresponds to a fully right-polarized phonon [11]. Special points in the Brillouin zone were selected following Ref. 48. The modes marked a–e are visualized in Fig. 4.

magnitudes vary widely between the calculations including a dispersion correction (Fig. 3) and calculations performed without it (see the Supplemental Material [30]). This discrepancy suggests that the qualitative level of accuracy in the calculated CTE (Table I) could be due to underestimation of the Grüneisen parameters of the chiral modes.

The relationship between phonon chirality and thermal expansion in  $\alpha$ - $\text{BiB}_3\text{O}_6$  can be understood further by examination of the chiral acoustic modes. If the structure of  $\alpha$ - $\text{BiB}_3\text{O}_6$  were achiral, in modes where Bi atoms revolve (*e.g.*, Fig. 4 c) adjacent Bi atoms would be required to revolve in opposite directions in order to maintain zero circular polarization [11, 12]. Therefore, modes which involve such revolutions are limited to the edges of the Brillouin zone in achiral crystals. As Fig. 3 shows, the modes that contribute most strongly to thermal expansion lie away from the edges of the Brillouin zone. This result indicates that revolutions of Bi atoms with small wavevectors couple strongly to the lattice strains, and if such phonons were disallowed by symmetry, the thermal expansion of  $\alpha$ - $\text{BiB}_3\text{O}_6$  would be less extreme.

Phonon chirality has previously been explored for potential applications in valleytronics [11–13], as chiral phonons can interact with valley electrons at the corners of the Brillouin zone in 2-dimensional chiral hexagonal materials. The present results therefore point to  $\alpha$ - $\text{BiB}_3\text{O}_6$  as a material which provides an avenues towards understanding of the effects of phonon chirality on the properties of 3-dimensional solids, due to its unusual and large-magnitude thermal expansion and the possibility of preparing large single crystals [17]. The calculations presented here have been obtained within the quasiharmonic

approximation; since phonon chirality changes the selection rules for three-phonon scattering [14] it could also affect the quartic contribution to the thermal expansion [50].

The chiral nature of  $\alpha$ - $\text{BiB}_3\text{O}_6$  is quite unusual among inorganic framework materials, and here the connection between that unusual structural feature and the phonons which cause anomalous thermal expansion has been revealed. It is interesting to note that, despite the general rarity of chiral inorganic crystals, several very prominent NTE materials crystallize in chiral space groups:  $\alpha$ - $\text{ZrW}_2\text{O}_8$ , which was the first material discovered to have isotropic NTE over a broad temperature range, crystallizes in  $P2_13$  [51], and  $\beta$ -eucryptite, which is the most widely used NTE material due to its inclusion in zero-thermal-expansion glass ceramics, crystallizes in  $P6_4222$  [52]. The structure of  $\beta$ -eucryptite is identical to that of  $\beta$ -quartz, which also displays NTE [53]. The relationship between phonon chirality and NTE is therefore a potentially fruitful topic for further study.

In conclusion, the vibrational origins of anomalous thermal expansion in  $\alpha$ - $\text{BiB}_3\text{O}_6$  have been investigated by *ab initio* calculation of the phonon band structure, elastic tensor, and mode Grüneisen parameters. Two types of phonon contribute significantly to thermal expansion: motions of the borate framework, and oscillations and revolutions of the bismuth atoms. These revolutions correspond to chiral acoustic phonons; along certain directions in reciprocal space the two transverse acoustic branches have opposite circular polarizations, with only one coupling strongly to the lattice strains. Were the lattice achiral, such rotations would be disallowed by symmetry except at the edges of the Brillouin zone, where they have small mode Grüneisen parameters. Anomalous thermal expansion in  $\alpha$ - $\text{BiB}_3\text{O}_6$  arises from these effects and is amplified by the low Young's moduli along **a** and **b**.

## ACKNOWLEDGEMENTS

The author acknowledges the support of the National Sciences and Engineering Council of Canada. Computational resources were provided by the University of Oxford, Department of Chemistry, and the UK's HEC Materials Chemistry Consortium, which is funded by EPSRC (EP/L000202). This work used the ARCHER UK National Supercomputing Service (<http://www.archer.ac.uk>).

---

\* [carl.romao@mnf.uni-tuebingen.de](mailto:carl.romao@mnf.uni-tuebingen.de)

[1] H. Hellwig, J. Liebertz, and L. Bohatý, Exceptional large nonlinear optical coefficients in the monoclinic bismuth

- borate  $\text{BiB}_3\text{O}_6$  (BIBO), *Solid State Commun.* **109**, 249 (1998).
- [2] O. Pinel, P. Jian, R. M. De Araujo, J. Feng, B. Chalopin, C. Fabre, and N. Treps, Generation and characterization of multimode quantum frequency combs, *Phys. Rev. Lett.* **108**, 083601 (2012).
- [3] L.-K. Chen, Z.-D. Li, X.-C. Yao, M. Huang, W. Li, H. Lu, X. Yuan, Y.-B. Zhang, X. Jiang, C.-Z. Peng, *et al.*, Observation of ten-photon entanglement using thin  $\text{BiB}_3\text{O}_6$  crystals, *Optica* **4**, 77 (2017).
- [4] X.-L. Wang, L.-K. Chen, W. Li, H.-L. Huang, C. Liu, C. Chen, Y.-H. Luo, Z.-E. Su, D. Wu, Z.-D. Li, *et al.*, Experimental ten-photon entanglement, *Phys. Rev. Lett.* **117**, 210502 (2016).
- [5] B. Teng, Z. Wang, H. Jiang, X. Cheng, H. Liu, X. Hu, S. Dong, J. Wang, and Z. Shao, Anisotropic thermal expansion of  $\text{BiB}_3\text{O}_6$ , *J. Appl. Phys.* **91**, 3618 (2002).
- [6] W.-D. Stein, A. Cousson, P. Becker, L. Bohatý, and M. Braden, Temperature-dependent X-ray and neutron diffraction study of  $\text{BiB}_3\text{O}_6$ , *Z. Krist.* **222**, 680 (2007).
- [7] L. Kang, X. Jiang, S. Luo, P. Gong, W. Li, X. Wu, Y. Li, X. Li, C. Chen, and Z. Lin, Negative linear compressibility in a crystal of  $\alpha$ - $\text{BiB}_3\text{O}_6$ , *Sci. Rep.* **5**, 13432 (2015).
- [8] A. B. Cairns and A. L. Goodwin, Negative linear compressibility, *Phys. Chem. Chem. Phys.* **17**, 20449 (2015).
- [9] C. P. Romao, K. J. Miller, C. A. Whitman, M. A. White, and B. A. Marinkovic, Negative thermal expansion (thermomimetic) materials, in *Comprehensive Inorganic Chemistry II* (Elsevier, 2013) pp. 127–151.
- [10] M. T. Dove and H. Fang, Negative thermal expansion and associated anomalous physical properties: review of the lattice dynamics theoretical foundation, *Rep. Prog. Phys.* **79**, 066503 (2016).
- [11] L. Zhang and Q. Niu, Chiral phonons at high-symmetry points in monolayer hexagonal lattices, *Phys. Rev. Lett.* **115**, 115502 (2015).
- [12] M. Gao, W. Zhang, and L. Zhang, Nondegenerate chiral phonons in graphene/hexagonal boron nitride heterostructure from first-principles calculations, *Nano Lett.* **18**, 4424 (2018).
- [13] H. Zhu, J. Yi, M.-Y. Li, J. Xiao, L. Zhang, C.-W. Yang, R. A. Kaindl, L.-J. Li, Y. Wang, and X. Zhang, Observation of chiral phonons, *Science* **359**, 579 (2018).
- [14] T. Pandey, C. A. Polanco, V. R. Cooper, D. S. Parker, and L. Lindsay, Symmetry-driven phonon chirality and transport in one-dimensional and bulk  $\text{Ba}_3\text{N}$ -derived materials, *Phys. Rev. B* **98**, 241405 (2018).
- [15] C. A. Kennedy and M. A. White, Unusual thermal conductivity of the negative thermal expansion material,  $\text{ZrW}_2\text{O}_8$ , *Solid State Commun.* **134**, 271 (2005).
- [16] R. Bubnova, S. Volkov, B. Albert, and S. Filatov, Borates—crystal structures of prospective nonlinear optical materials: High anisotropy of the thermal expansion caused by anharmonic atomic vibrations, *Crystals* **7**, 93 (2017).
- [17] A. Egorysheva and V. Skorikov, Efficient nonlinear optical material  $\text{BiB}_3\text{O}_6$  (BIBO), *Inorg. Mater.* **45**, 1461 (2009).
- [18] A. L. Goodwin, M. Calleja, M. J. Conterio, M. T. Dove, J. S. O. Evans, D. A. Keen, L. Peters, and M. G. Tucker, Colossal positive and negative thermal expansion in the framework material  $\text{Ag}_3[\text{Co}(\text{CN})_6]$ , *Science* **319**, 794 (2008).



- [19] M. S. Senn, A. Bombardi, C. A. Murray, C. Vecchini, A. Scherillo, X. Luo, and S. W. Cheong, Negative thermal expansion in hybrid improper ferroelectric Ruddlesden-Popper perovskites by symmetry trapping, *Phys. Rev. Lett.* **114**, 035701 (2015).
- [20] E. T. Ritz and N. A. Benedek, Interplay between phonons and anisotropic elasticity drives negative thermal expansion in pbtio 3, *Phys. Rev. Lett.* **121**, 255901 (2018).
- [21] C. P. Romao, F. A. Perras, U. Werner-Zwanziger, J. A. Lussier, K. J. Miller, C. M. Calahoo, J. W. Zwanziger, M. Bieringer, B. A. Marinkovic, D. L. Bryce, and M. A. White, Zero thermal expansion in  $\text{ZrMgMo}_3\text{O}_{12}$ : NMR crystallography reveals origins of thermoelastic properties, *Chem. Mater.* **27**, 2633 (2015).
- [22] C. P. Romao, Anisotropic thermal expansion in flexible materials, *Phys. Rev. B* **96**, 134113 (2017).
- [23] S. Bhattacharya and B. K. Saha, Uniaxial negative thermal expansion in an organic complex caused by sliding of layers, *Cryst. Growth & Des.* **12**, 4716 (2012).
- [24] B. K. Saha, Thermal expansion in organic crystals, *J. of the Indian Inst. Sci.* **97**, 177 (2017).
- [25] M. Baise, P. M. Maffettone, F. Trouselet, N. P. Funnell, F.-X. Coudert, and A. L. Goodwin, Negative hydration expansion in  $\text{ZrW}_2\text{O}_8$ : Microscopic mechanism, spaghetti dynamics, and negative thermal expansion, *Phys. Rev. Lett.* **120**, 265501 (2018).
- [26] X. Gonze, F. Jollet, F. A. Araujo, D. Adams, B. Amadon, T. Applencourt, C. Audouze, J.-M. Beuken, J. Bieder, A. Bokhanchuk, *et al.*, Recent developments in the ABINIT software package, *Comp. Phys. Comm.* **205**, 106 (2016).
- [27] F. Bottin, S. Leroux, A. Knyazev, and G. Zerah, Large-scale ab initio calculations based on three levels of parallelization, *Comp. Mater. Sci.* **42**, 329 (2008).
- [28] T. Björkman, CIF2cell: generating geometries for electronic structure programs, *Comp. Phys. Commun.* **182**, 1183 (2011).
- [29] M. Torrent, F. Jollet, F. Bottin, G. Zerah, and X. Gonze, Implementation of the projector augmented-wave method in the ABINIT code: Application to the study of iron under pressure, *Comp. Mater. Sci.* **42**, 337 (2008).
- [30] See Supplemental Material for example DFT input files, further description of computational methods, elastic tensors, mode Grüneisen parameters calculated without dispersion correction, and phonon polarizations. Additionally, animations of several important phonon modes and phonon eigenvectors in JSON format can be downloaded from <https://bit.ly/2V83qSu>.
- [31] X. Gonze and C. Lee, Dynamical matrices, Born effective charges, dielectric permittivity tensors, and interatomic force constants from density-functional perturbation theory, *Phys. Rev. B* **55**, 10355 (1997).
- [32] B. Van Troeye, M. Torrent, and X. Gonze, Interatomic force constants including the DFT-D dispersion contribution, *Phys. Rev. B* **93**, 144304 (2016).
- [33] W. Kohn and L. J. Sham, Self-consistent equations including exchange and correlation effects, *Phys. Rev.* **140**, A1133 (1965).
- [34] L. He, F. Liu, G. Hautier, M. J. Oliveira, M. A. Marques, F. D. Vila, J. Rehr, G.-M. Rignanese, and A. Zhou, Accuracy of generalized gradient approximation functionals for density-functional perturbation theory calculations, *Phys. Rev. B* **89**, 064305 (2014).
- [35] S. Grimme, J. Antony, S. Ehrlich, and H. Krieg, A consistent and accurate ab initio parametrization of density functional dispersion correction (DFT-D) for the 94 elements H-Pu, *J. Chem. Phys.* **132**, 154104 (2010).
- [36] A. D. Becke and E. R. Johnson, A simple effective potential for exchange, *J. Chem. Phys.* **124**, 221101 (2006).
- [37] J. P. Perdew, K. Burke, and M. Ernzerhof, Generalized gradient approximation made simple, *Phys. Rev. Lett.* **77**, 3865 (1996).
- [38] D. R. Hamann, Optimized norm-conserving Vanderbilt pseudopotentials, *Phys. Rev. B* **88**, 085117 (2013).
- [39] H. J. Monkhorst and J. D. Pack, Special points for Brillouin-zone integrations, *Phys. Rev. B* **13**, 5188 (1976).
- [40] psp tables — ABINIT, <https://www.abinit.org/psp-tables>, accessed: 2017-01-20.
- [41] SG15 ONCV potentials, [http://www.quantum-simulation.org/potentials/sg15\\_oncv/](http://www.quantum-simulation.org/potentials/sg15_oncv/), accessed: 2017-01-20.
- [42] R. Gaillac, P. Pullumbi, and F.-X. Coudert, ELATE: an open-source online application for analysis and visualization of elastic tensors, *J. Phys.: Condens. Matter* **28**, 275201 (2016).
- [43] L. H. N. Rimmer, M. T. Dove, A. L. Goodwin, and D. C. Palmer, Acoustic phonons and negative thermal expansion in MOF-5, *Phys. Chem. Chem. Phys.* **16**, 21144 (2014).
- [44] H. Fang, M. T. Dove, and A. E. Phillips, Common origin of negative thermal expansion and other exotic properties in ceramic and hybrid materials, *Phys. Rev. B* **89**, 214103 (2014).
- [45] A. U. Ortiz, A. Boutin, A. H. Fuchs, and F.-X. Coudert, Anisotropic elastic properties of flexible metal-organic frameworks: How soft are soft porous crystals?, *Phys. Rev. Lett.* **109**, 195502 (2012).
- [46] A. U. Ortiz, A. Boutin, A. H. Fuchs, and F.-X. Coudert, Metal-organic frameworks with wine-rack motif: What determines their flexibility and elastic properties?, *J. Chem. Phys.* **138**, 174703 (2013).
- [47] K. Dolabdjian, A. Kobald, C. P. Romao, and H.-J. Meyer, Synthesis and thermoelastic properties of  $\text{Zr}(\text{CN}_2)_2$  and  $\text{Hf}(\text{CN}_2)_2$ , *Dalton Trans.* **47**, 10249 (2018).
- [48] Y. Hinuma, G. Pizzi, Y. Kumagai, F. Oba, and I. Tanaka, Band structure diagram paths based on crystallography, *Comp. Mater. Sci.* **128**, 140 (2017).
- [49] Phonon visualization website, <http://henriquemiranda.github.io/phonon-visualization-website.html>, accessed: 2018-11-16.
- [50] D. S. Kim, O. Hellman, J. Herriman, H. L. Smith, J. Y. Y. Lin, N. Shulumba, J. L. Niedziela, C. W. Li, D. L. Abernathy, and B. Fultz, Nuclear quantum effect with pure anharmonicity and the anomalous thermal expansion of silicon, *Proc. Natl. Acad. Sci.* **115**, 1992 (2018).
- [51] T. A. Mary, J. S. O. Evans, T. Vogt, and A. W. Sleight, Negative thermal expansion from 0.3 to 1050 Kelvin in  $\text{ZrW}_2\text{O}_8$ , *Science* **272**, 90 (1996).
- [52] A. I. Lichtenstein, R. O. Jones, H. Xu, and P. J. Heaney, Anisotropic thermal expansion in the silicate  $\beta$ -eucryptite: A neutron diffraction and density functional study, *Phys. Rev. B* **58**, 6219 (1998).
- [53] P. R. L. Welche, V. Heine, and M. T. Dove, Negative thermal expansion in beta-quartz, *Phys. Chem. Minerals* **26**, 63 (1998).